Heliyon 10 (2024) e29577

Contents lists available at ScienceDirect

Heliyon

journal homepage: www.cell.com/heliyon

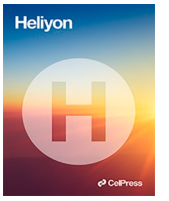

Research article

Influence of the internal structure of straight microchannels on inertial transport behavior of particles

Hua Dong [a,*], Longrun Huang [b], Liang Zhao [a]

[a] State Key Laboratory of Multiphase Flow in Power Engineering, Xi'an Jiaotong University, Xi'an, 710049, PR China
[b] School of Mechanical Engineering, Xi'an Jiaotong University, Xi'an, 710049, PR China

ARTICLE INFO

Keywords:
Reynolds number
Particle
Microchannel
Biomedicine

ABSTRACT

The rapid advancement of Micro-Electro-Mechanical Systems (MEMS) technology has established microfluidics as a pivotal field. This technology marks the onset of a new era in various applications, including drug testing, cell culture, and disease monitoring, underscoring its extensive practicality and potential for future exploration. This research delves into the intricate behavior of particle inertial migration within microchannels, particularly focusing on the impact of different channel structures and Reynolds numbers (R_e). Our studies reveal that particles in microchannels with one-sided sharp-cornered microstructures migrate towards the sharp corner at a relative position of 0.4 under low flow rates, and towards the straight wall side at a relative position of 0.8 under high flow rates. The migration pattern of equilibrium positions varies with different arrangements of sharp-corner structures, achieving stability at the channel's center only when the sharp corners are symmetrically arranged on both sides. Our investigation into the shape of microstructures indicates that sharp-cornered structures generate a more stable secondary flow compared to rectangular and semi-circular structures, preventing particle aggregation at the outlet. To address the challenges associated with handling variable cross-section geometries and solid-wall boundaries in dissipative particle dynamics methods effectively, we have developed a dissipative particle dynamics model specifically for analyzing such microchannels. Building upon our previous research, this model introduces a conservative force coefficient for particles within the microstructured region and an interaction zone that only involves repulsive forces, aligning well with experimental outcomes. Through the study of microstructures' geometric shapes, this paper offers guidance for designing microchannels for particle enrichment. Furthermore, the dissipative particle dynamics model established for the particle flow and solid structure interaction within microstructured channels provides insights into the mesoscale dynamics of liquid-solid two-phase flow and particle motion. In conclusion, this paper aims to enhance particle motion sample preparation techniques, thereby broadening the scope of microfluidic applications in the biomedical field.

* Corresponding author.
E-mail address: cvvdonghua@sina.com (H. Dong).

https://doi.org/10.1016/j.heliyon.2024.e29577
Received 16 December 2023; Received in revised form 9 April 2024; Accepted 10 April 2024
Available online 14 April 2024

1. Introduction

1.1. Background

With the rapid development of micro electro mechanical system (MEMS) technology, micro cells with biomedical sample processing function can be manufactured and integrated into chips. Therefore, the concept of "lab on chip" [1] (also known as micro total analysis system or microfluidic chip) was proposed. The first appearance of microfluidic technology is believed to be in the 1990s. Since then, it has experienced exponential growth and has become a powerful analytical tool with great development potential integrating sample preparation, mixing, reaction, separation, cell culture, sorting, splitting and detection [2]. Microfluidic technology has the advantages of less sample demand, fast processing speed, high processing accuracy, small size, good flexibility and low cost. In view of its highly integrated characteristics, microfluidic chips may gradually supplement or even replace existing analytical equipment [3]. The increasing application potential of microfluidic technology brings new perspectives to academic and industrial sectors. In addition, this technology is also very promising in daily application. Some commercially available devices have been used for rapid detection of coronavirus and blood glucose monitoring [4,5].

On the basis of microfluidic chips, efficient sample pretreatment can greatly improve the performance of the microanalysis system [6]. At present, the sample pretreatment technologies such as sample mixing, enrichment and separation are realized through the manipulation of microfluidics, which are widely used in drug detection, cell culture, organ chip, disease monitoring and many other fields, and have broad application prospects [7–18].

In the 1960s, Segre and Sliberberg first found that particles in small-scale channels with circular cross section would gradually migrate to about 0.6 times the channel radius and form narrow annular enrichment zones [19]. Kim et al. [20] studied the lateral migration of particles at different channel blockage ratios, and also found that the particle balance is 0.6 times the channel radius. Matas team [21] studied the particle movement in Poiseuille flow in a circular pipe, and found that when R_e is small, the particles move towards the annular wall, but when R_e exceeds 600, the particles form an internal ring that is balanced at less than 0.6 times the radius. Domestic and foreign scholars have developed microfluidic technology for particle movement control based on the research on the lateral migration behavior of particles in microchannels.

In the realm of particle enrichment research within straight channels, simple structures sensitive to flow variations have been predominantly explored, as evident in the works of Hur [22] and Hasson [23]. Park et al. [24] innovatively incorporated contraction and expansion structures in microchannels, optimizing particle focusing through secondary flow and inertial lift. However, this method resulted in a broad enrichment bandwidth. Other studies, like those by Yilmaz et al. [25] and Lee et al. [26], utilized various contraction-expansion configurations, achieving successful particle and RBC enrichment, albeit at varied flow rates and efficiencies. Zhang et al. [27] and Chung et al. [28] introduced intricate designs, generating multifaceted secondary flows and creating platforms for enhanced inertial focusing of particles and cells. Yuan et al. [29] advanced this field further by achieving high-purity plasma extraction utilizing a sophisticated ECCA channel design. In our previous contributions [30], we proposed a unique microchannel featuring asymmetric sharp corner structures, which facilitated highly concentrated, single-particle flows across a diverse flow velocity range, marking a notable enhancement in channel design and particle enrichment processes.

In addition, numerical simulation is also widely used as another means to study particle motion in microchannels [31,32]. Among the mesoscopic scale numerical simulation methods, the dissipative particle dynamics (DPD) method and lattice Boltzmann (LB) method can well solve the micro scale flow problems. LB method has simple algorithm and high calculation efficiency, and can simulate various complex nonlinear macroscopic phenomena. The DPD method combines the advantages of molecular dynamics and lattice Boltzmann method to study the particle flow problem at the mesoscopic level through coarsening, which not only considers the interaction between particles, but also saves computing resources and improves computing efficiency [33,34].

At present, the study on the solid wall boundary treatment method of DPD is only found in simple channels. Some scholars use frozen DPD particles as solid walls. These frozen particles are still at a fixed position and interact with fluid particles. However, this method of solid wall boundary treatment cannot prevent fluid particles from passing through solid walls [35–41].In our prior research [42], our team strategically utilized two frozen layers of DPD particles to represent the wall boundaries. By meticulously adjusting the simulation parameters, we managed to modify the Schmidt number, thereby enhancing the simulation's fidelity in mirroring the authentic physical properties of water. This refined approach enabled us to successfully simulate the lateral migration of microparticles within the Newtonian fluid flow inside microchannels, marking a significant advancement in our understanding and manipulation of microfluidic phenomena.

1.2. Objectives of the study

In conclusion, the microchannel's geometric structure crucially influences particles' inertial focusing, impacting the precision of particle motion control. Understanding the channel structure's effect on particle inertial migration is fundamental to realizing efficient particle motion control in microfluidic technology. Current studies primarily focus on microchannels with periodic straight geometry for inertial particle focusing, leaving the influence of variable cross-section structures underexplored and unclear. In channels with a specific aspect ratio, particles experience an inertial lift force (F_i) that is comprised of the shear gradient lift force (F_{LS}) and the wall effect lift force (F_{LW}). Particles moving alongside the center of the channel are propelled towards the walls due to the shear gradient lift, whereas those near the walls are nudged towards the center by the wall effect lift. This results in particles eventually aligning themselves at the channel's center (specifically at the center of the long walls in the cross-section) as a balance is achieved between these forces. In the unique straight microchannels with varying cross-sectional structures presented in this study, the side-to-side

movement of particles is governed by a competitive interplay among the inertial lift force (F_i), viscous drag force (F_d), and an inertial centrifugal force (F_c) prompted by the changes in the microchannel's cross-sectional geometry. Therefore, this study systematically demonstrates the influence of microchannel geometric structures on particle inertial migration and validates it through experiments and simulations, which will propel the development of microfluidic technology applications in biomedicine, chemical analysis, and detection.

Furthermore, the existing macroscopic continuum models fall short of capturing the microscopic nuances of particle motion in microchannels. While the dissipative particle dynamics (DPD) method has advanced the study of particle motion in microchannels, research focusing on slip-free solid wall boundary conditions in straight channels is more established. However, an effective method to address the solid wall boundaries in variable cross-section structure channels is lacking. It necessitates developing suitable DPD models and solid wall boundary treatment methods for these channels, aiming to enhance the mesoscopic scale research of particle motion in complex structural channels. In this study, by increasing the Schmidt number in the DPD simulations, which elevates the ratio of momentum transfer speed to mass transfer speed to match the physical properties of real water, and enhancing the conservative force coefficient among particles in the microstructured region, an interaction zone featuring only repulsive forces was introduced. This approach effectively addresses the challenge of dealing with solid wall boundaries in variable cross-section geometries encountered in dissipative particle dynamics methods. By comparing with experimental results, the lateral movement patterns and trends of particles showed good agreement with the experiments.

1.3. Working principle

In conventional scale channels, due to the large difference between particle size and channel hydraulic diameter, R_{ep} is far less than 1. At this time, the lateral movement of particles is caused by Magnus force and Saffman force [43]. However, under the microscale condition, the difference between the particle size and the hydraulic diameter of the channel is small, and R_{ep} is usually not less than 1. The force analysis of particle movement under the macro scale is no longer applicable to the lateral movement of particles in the microchannel. Therefore, it is necessary to analyze the dynamics of particle movement in microchannels. Because the particles in the flow bear the shear stress and normal stress on their surfaces at the same time, the forces parallel to the main flow direction (i.e. resistance) and perpendicular to the main flow direction (i.e. lift) are generated.

1.3.1. Dean drag force

When an object passes through a fluid, or relatively, when a fluid passes through an object, there is resistance. In the microchannel, in most flows, the viscous drag force will play a role in accelerating particles, allowing particles to follow the streamline. The viscous drag force (F_d) on the moving spherical particles can be expressed as Equation (1):

$$F_d = 3\pi\mu a_p U_s \tag{1}$$

Where: μ —— Fluid viscosity coefficient/N·s·m^{-2}; a_p ——particle size/m; U_s —— relative velocity of fluid and particles/m·s^{-1}. As a case similar to viscous drag force, Dean vortex [44] will be generated on the cross section in the bending channel, and particles will be dragged by Dean vortex in the bending channel, that is, Dean drag force (F_D). The formula is as follows [45] shown in:Equation 2.

$$F_D = 3\pi\mu a_p U_D \tag{2}$$

Where: U_D —— average Dean speed/m·s^{-1}.

1.3.2. Inertial lift

Inertial lift (F_i) can be divided into shear gradient lift (F_{LS}) and wall action lift (F_{LW}). The wall effect lift (F_{LW}) is caused by the wall viscosity and the asymmetric eddy current on the particle surface. The effect of the wall effect lift on the puppet motion is to slow down the ball's motion and repel the particles to the centerline of the channel. The existence of the wall will produce the velocity gradient (shear rate) of the fluid. Because the particles in the channel are subject to different velocity distributions on both sides, shear gradient lift (F_{LS}) will be generated. Under the action of the shear gradient lift, the particles will migrate to the wall. Therefore, under the combined action of two lifting forces, namely, inertial lifting force, particles will migrate laterally to the equilibrium position in the channel [46]. The inertial lift expression is as follows shown in Equation (3):

$$F_i = C_L \rho_f G^2 a_p^4 \tag{3}$$

Where: C_L —— inertial lift coefficient; ρ_f —— fluid density/Kg·m^{-3}; G —— fluid shear rate/s^{-1}.

1.3.3. Saffman lift

The existence of the wall will produce the velocity gradient (shear rate) of the fluid, resulting in the Saffman lift (F_{saff}) generated by the sliding shear of the spherical particles. When the particle movement is ahead of the fluid, the Saffman lift will push the particles to the walls on both sides. When the particles lag behind the fluid, the Saffman lift effect will cause the particles to migrate to the center. The Saffman lift expression is as follows [47] shown in Equation (4):

$$F_{saff} = 6.46 a_p \mu R_G(r)^{1/2} U_s \tag{4}$$

Where: R_G *(r)* —— dimensionless particle Reynolds number based on local shear rate. When $R_{ep} \ll 1$, the above formula is valid [48].

1.3.4. *Magnus lift*

The existence of the wall will produce the velocity gradient (shear rate) of the fluid, which will lead to the sliding rotation of spherical particles. For particles rotating in the fluid, due to the lateral pressure difference, there will be a lateral lift, which is called Magnus force (F_M), and the expression is as follows [49] shown in Equation (5):

$$F_M = \pi a_p^3 \rho_f \omega U_s \tag{5}$$

Where: ω —— Angular velocity of particles/rad·s^{-1}.

For particles moving in a linear microchannel, in addition to the viscous drag force F_d along the flow direction, there are four lateral forces acting on the particles: Magnus lift generated by sliding rotation, Saffman lift generated by sliding shear, wall lift F_{LW} caused by the disturbance of the flow field around the particles from the wall, and shear gradient lift F_{LS} caused by the curvature of the undisturbed fluid velocity profile. Among them, since the Magnus lift and Saffman lift generated by shear are often much smaller than the shear gradient lift, they can be ignored. The shear gradient lift that leads particles to the channel wall and the wall lift that pushes particles to the center line of the channel, namely the inertial lift F_i, are generally considered as the main effects of particle lateral migration [50]. Particle Reynolds number (R_{ep}) is usually used to characterize the lateral migration of particles in the straight passage. It describes the ratio of inertial force and viscous force of fluid in the flow, and its expression is as follows shown in Equation (6):

$$R_{ep} = \frac{\rho_f U_M a_p^2}{\mu D_h} \tag{6}$$

Where: U_m —— maximum velocity of fluid/m·s^{-1}; D_h —— hydraulic diameter of channel/m. When $R_{ep} \ll 1$, particles are mainly subjected to viscous drag force to follow the fluid streamline.However, when R_{ep} increases to the order of 1, the inertial lift is dominant, and the lateral migration of particles on the fluid streamline becomes obvious. By balancing the inertial lift and viscous drag on particles in the microchannel, the lateral migration velocity of particles in the straight channel, U_L, can be obtained shown in Equation (7):

$$U_L^2 \propto \frac{C_L \rho_f G^2 a_p^3}{3\pi\mu} \tag{7}$$

It can be seen that the lateral velocity of particles in the microchannel is directly determined by the channel geometry ($G = U_m/D_h$). And based on the previous research of the research group, the introduction of sharp angle structure in the straight passage can trigger the effect of inertial centrifugal force (F_c), and achieve the enrichment of a single particle chain. Therefore, in this paper, the control effect of inertial centrifugal force on the lateral movement of particles in the microchannel is coupled, and a microchannel with variable cross-section structure is designed. When particles flow through the variable cross-section structure, their momentum changes, which will lead to inertial centrifugal force, thus regulating the lateral movement of particles.

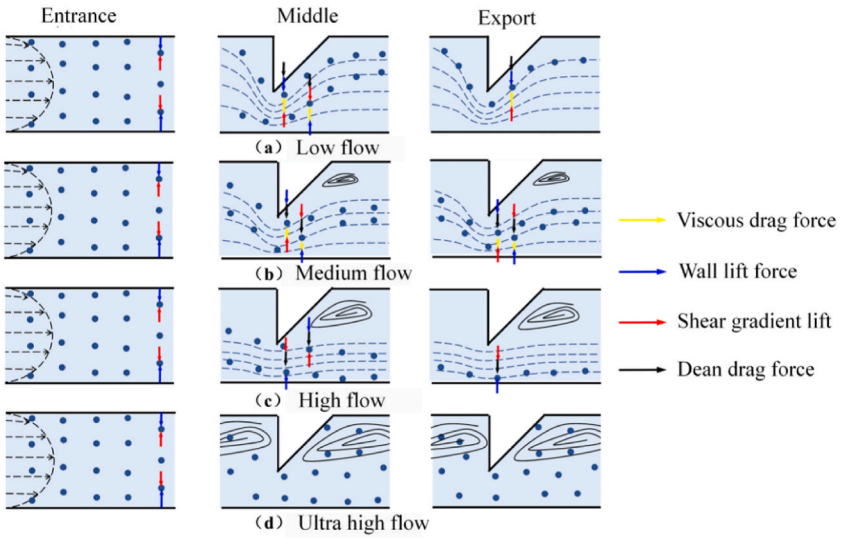

Fig. 1. Schematic diagram of particle lateral movement in linear microchannel with microstructure.(a) Schematic of particle lateral movement in a straight microchannel with microstructures under low flow rates. (b) Schematic of particle lateral movement in a straight microchannel with microstructures under medium flow rates (c) Schematic of particle lateral movement in a straight microchannel with microstructures under high flow rates. (d) Schematic of particle lateral movement in a straight microchannel with microstructures under very high flow rates.

In a straight passage with a certain aspect ratio, the inertial lift (F_i) can be divided into two components: shear gradient lift (F_{LS}) and wall action lift (F_{LW}). Particles moving on both sides of the channel center will move toward the wall under the action of shear gradient lift, while particles moving near the walls on both sides will migrate toward the channel center under the action of wall lift. Finally, under the balance of the two components, particles will finally focus on the center of the channel (the center of the long wall on the section) by inertia. In the linear microchannel with variable cross-section structure designed in this paper, the lateral motion of particles is determined by the competition mechanism between the inertial lift (F_i), viscous drag (F_d) and the inertial centrifugal force (F_c) caused by the variable cross-section microstructure. When the flow velocity is low (Fig. 1(a)), the inertial centrifugal force is less than the inertial lift [30], and R_{eP} is in the order of 1. Particles are mainly affected by inertial lift and viscous drag force. Under the effect of inertial lift, particles reach a specific inertial equilibrium position in the channel. The introduction of variable cross-section microstructure can induce curved streamline, Under the action of the lateral component of the viscous drag force in the sharp corner structure area, the particles will follow the curved streamline to migrate to the sharp corner side, thus modifying the inertial balance position of the particles. Finally, through a series of sharp corner structures, all particles will finally reach the new balance position of the force balance on the side of the microstructure, and a particle belt will be rich on the side of the microstructure at the outlet of the channel. When the flow is further increased to medium flow (Fig. 1(b)), the inertial centrifugal force and inertial lift caused at the sharp corner are equivalent [30], while R_{eP} is on the order of 10, and the viscous drag force is less than the inertial lift by an order of magnitude, which is ignored. Therefore, under the driving action of the inertial centrifugal force, the particles originally balanced at the side of the microstructure gradually migrate to the straight channel wall. At this time, due to the small difference in magnitude between the inertial centrifugal force and the inertial lift force, the particles finally migrate laterally to multiple positions in the channel, and multiple particle flows appear. When the flow rate increases to high flow rate again (Fig. 1(c)), the inertial centrifugal force caused at the microstructure is far greater than the inertial lift force. Driven by the strong inertial centrifugal force, after passing through a series of microstructures, all particles are driven to the vicinity of the straight wall, and the particles are balanced by the inertial centrifugal force and inertial lift force, so that the particles form a single particle flow at this equilibrium position. However, if the flow rate is further increased to the ultra-high level (Fig. 1(d)), the inertial lift is dominant [30], but there will be large eddy currents in the expansion area, and the flow may be excessive to turbulence, and the particles begin to move randomly. Here and throughout the work, the definition of "equilibrium" or "equilibrium position" does not mean that the system is in equilibrium in the thermodynamic sense, but refers to the mathematical definition of particles occupying the static point of the dynamic system.

2. Design and fabrication of microchannel

In this paper, the control effect of inertial centrifugal force on the lateral movement of particles in the microchannel is coupled, and a microchannel with variable cross-section structure is designed. When particles flow through the variable cross-section structure, their momentum changes, which will lead to inertial centrifugal force, thus regulating the lateral movement of particles. In this paper, four kinds of variable cross-section micro structure straight channels are designed, including rectangular, arc, semicircle and cusp structure micro channels, and different cusp forms are further considered (as shown in Fig. 2), including the entrance width at the dimensionless cusp ($W_s' = 1\text{-}W_s/W$) of 0.25, 0.375, 0.5, 0.627, 0.75 and 0.875 respectively; Dimensionless corner spacing ($L_d'=L_d/W_s$) is 1.5, 2.5, 4, 5, 7.5 respectively; The dimensionless channel width ($W'=W/W_s$) is 2, 3, 4, 5, 6 respectively; The arrangement of sharp corners is staggered, symmetrical and unilateral.

The overall structure of the microchannel is shown in Fig. 3 The channel consists of inlet A, observation area B, functional segment microstructure channel area C, and outlet D. The inlet and outlet of the channel are cylinders with a diameter of 2 mm, and the channel depth is 30 μm. It is convenient to capture the distribution of particles at the outlet of the inlet channel, and the width of the observation area is 800 μm. The functional segment length (L) is composed of 80 identical microstructures. See Table 1 for specific dimensions of microchannel.

In this paper, Polydimethylsiloxane (PDMS Dow Corning, USA) materials are selected to make microchannels for this study. The standard soft lithography technology with high machining accuracy is selected to fabricate the microchannel designed in this paper. Standard soft lithography process flow [51], including mask design and preparation, rotary coating production of photoresist, exposure development and channel size calibration, mold turnover and drilling, and microchannel bonding process.

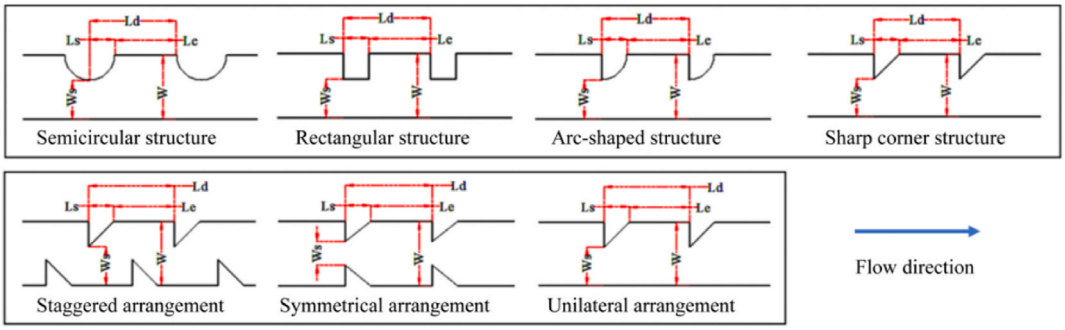

Fig. 2. Schematic diagram of the functional segment of the micro structure channel.

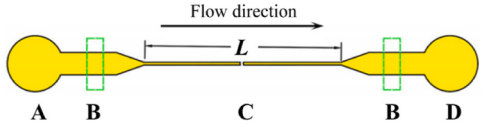

Fig. 3. Overall schematic diagram of microstructure channel.

Table 1
Specific dimensions of the microstructural channels used in the study.

Research factors	Channel structure parameters (sharp angle is 45°)
Microstructure shape	$W_s = 40$ μm;$L_s = 40$ μm; $L_e = 120$ μm; $W = 80$ μm; Unilateral arrangement
Sharp angle arrangement	$W_s = 40$ μm; $L_d = 200$ μm; $W = 80$ μm

3. Experimental methods

In this experiment, the continuous phase is deionized water, and the particle size is 10 μ M standard polystyrene spherical particles (Suzhou Nanotech Co., Ltd.), particle density is 1.062×10^3 kg m^{-3}, particle size distribution deviation is less than 2.41 %. When preparing the particle solution, put the particle stock solution into the ultrasonic cleaner for ultrasonic bath to make the particles disperse evenly in the stock solution. After that, use a liquid transfer gun to mix a certain amount of particle stock solution with a certain amount of deionized water to configure the particle concentration required for experimental research. In order to prevent agglomeration between particles, 0.5 wt percent(wt%) Tween 20 surfactant solution (Shanghai Sinopharm Chemical Reagent Co., Ltd.) was added to the particle solution. At the beginning of the experiment, it is also necessary to shake the prepared particle solution again to ensure that the particles are completely dispersed, so as to improve the accuracy of the experiment. In the experiment, the solution concentration is (0.8–1.1) per microliter of particle solution $\times 10^4$ polystyrene particles, flow range: 50 μL min^{-1}, 100 μL min^{-1}, 200 μL min^{-1} to 600 μL min^{-1}。

The visual microfluidic experiment platform consists of a micro injection pump, a syringe, a PTFE hose, a microfluidic chip, a microscope, a high-speed camera and a computer. It is divided into two systems: flow drive control and experimental image capture. In the flow drive control system, the micro injection pump passes the sample solution in the syringe through the polytetrafluoroethylene hose to the micro channel inlet. The experimental image capture system uses a high-speed camera, microscope and computer to observe and photograph the fluid flow and particle movement in the microchannel. The specific information is shown in Table 2.

The specific steps of the experimental operation are as follows.

(1) Place the microchannel fabricated from PDMS (Dow Corning, USA) through photolithography under the microscope and secure it. Adjust the microscope's focus and the high-speed camera settings so that the structure of the microchannel can be clearly observed. Then, draw deionized water with a syringe, mount the syringe on the microinjection pump, and connect the syringe to the microchannel inlet with a PTFE hose.
(2) Adjust the flow rate of the microinjection pump to inject deionized water into the microchannel. After waiting for 5 min, observe through the microscope for any leaks, blockages, or bubbles in the entire microchannel. If there are no abnormalities, remove the syringe and replace it with one containing the sample solution. Before connecting it to the microchannel inlet, first, ensure that air bubbles are expelled from the syringe and hose.
(3) Adjust the microinjection pump to the flow rate required for the experiment. Four minutes after injecting the sample solution into the channel, check for leaks, blockages, and bubbles. If everything is normal, use the high-speed camera to capture the necessary experimental images. Additionally, wait for 5 min before adjusting the flow rate each time to allow the pressure inside the channel to stabilize again.
(4) After completing all conditions, remove the sample solution syringe and inject deionized water into the microchannel for cleaning. Then, seal the channel inlet and outlet with tape for future experimental use. Next, save and copy the experimental data, and turn off the high-speed camera, microscope, and computer.

The inherent differences between experimental outcomes and their true values are inevitable due to objective conditions and operator actions. An uncertainty analysis of these results is crucial for quantifying the extent and range of this discrepancy, facilitating

Table 2
Table of experimental instrument parameters.

Name of experimental instrument	Model	Manufactor
Disposable sterile syringe	5 ml	Honghu Taining Medical Instrument Co., Ltd
Microinjection pump	KDS200	KD Scientific
CCD Camera	FASTCAM Mini UX1000	Photron FASTCAM
Microscope	DM4000B	Leica MICROSYSTEMS

an objective and scientific appraisal of the findings. Such analysis is also instrumental in refining experimental methodologies, thereby enhancing the precision and trustworthiness of the measurements obtained.

In the course of this study, identified sources of uncertainty include the flow rate error associated with the microinjection pump and the deviation in particle sizes. The experiments were conducted using a KDS200 microinjection pump, which offers a minimum flow rate capability of 1 μL h^{-1}. Given that the flow rates employed in these experiments are measured in μL·min^{-1}, the uncertainty attributed to the pump's flow rate is determined to be less than 1 %. This minimal uncertainty, especially within the context of liquid-liquid two-phase flow studies, underscores the advantage of employing a single pump drive over dual pump systems, which are prone to cumulative uncertainty issues, thus bolstering the reliability of our experimental findings.

The particles utilized in the experiment were standard polystyrene spherical particles supplied by Suzhou Nano Micro Technology Co., Ltd., with a density of 1.062×10^3 kg m^{-3}. The uncertainty in particle size distribution was ascertained to be less than 2.41 %. Based on the analysis presented, we can affirm that the experimental data garnered from the employed microfluidic visualization platform is dependable, providing a solid basis for the conclusions drawn in this study.

In this paper, Getdata (GetData. AUS) software is used to analyze the lateral distribution of particles, as shown in Fig. 4.

In order to clearly characterize the particle position, the channel width (W) is dimensionless in this paper. The channel center is the benchmark ($z = 0$), and the upper and lower walls of the channel (one side of the microstructure) are $z = 1$ and $z = -1$ respectively. In this way, the dimensionless lateral relative position of each particle from the channel center can be obtained.

In order to obtain the distribution of particles in the channel. In this paper, the channel width is divided into 40 intervals, the number of particles in each interval is counted, and the ratio to the total number in the whole sampling area is the enrichment factor $f(k)$. The calculation formula is as follows:

$$f(k) = \frac{N_k}{\sum_{k=1}^{k=40} N_k} \tag{8}$$

$$\overline{z} = \sum_{k=1}^{k=40} |\overline{z}_k| \cdot f(k) \tag{9}$$

4. Results and discussion

4.1. Inertial migration dynamics of particles in linear microchannels featuring integrated microstructures

Firstly, the influence of angular structure arrangement on the inertial transport behavior of particles is studied. The angular structure distribution forms are unilateral distribution, symmetric distribution and bilateral staggered distribution.

Under different flow conditions, The distribution of 10 μm particles at the outlet of the sharp corner structure microchannel with different arrangements is shown in Fig. 5. In order to further understand the inertial migration characteristics of particles in the microchannels with different angular structures, the particle distribution at the outlet of the channel is counted. The particle distribution histogram at the outlet of the channel with different angular structures is shown in Fig. 6.

Fig. 5 (b) and 6 (b) show that when the sharp corner structure is symmetrically arranged, the equilibrium position of particles is always distributed in the center of the channel in the entire flow range, but with the increase of flow, the particle distribution bandwidth will become larger. This is because in the symmetrical angular structure microchannel and the low flow range of 50–100 μL min^{-1} (R_e is 23.8–47.6), the Dean drag force on both sides is offset, and the particles are balanced in the center of the channel under the action of inertial lift. As the flow increases to 200 μL min^{-1} ($R_e = 95.2$) or above, the effect of Dean's drag force will be enhanced, and the resultant force of Dean's drag force caused by symmetrical distribution of sharp angle structure will push the particles toward the center of the channel, so the inertial balance position at the center of the channel generated by inertial lift will not be modified to form a single particle flow. Figs. 5(c) and 6(c) show that when the sharp angle structure is staggered on both sides, when the flow rate is lower than 50–100 μL min^{-1} (R_e is 23.8–47.6), particles will be enriched into a particle flow in the center of the channel. This is because the particles are offset by Dean's drag force when passing through two interlaced sharp angle structures in turn, so the particles are mainly affected by the inertial lift and distributed at the inertial balance position in the center of the channel, forming an enrichment zone at the center of the channel outlet. As the flow increases to 200 μL min^{-1} or above, particles begin to migrate to both sides of the channel. This is because with the increase of the flow rate, the effect of particles under Dean's drag force will increase and

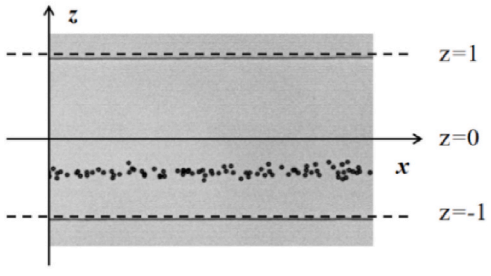

Fig. 4. Experimental image coordinate of particle lateral movement.

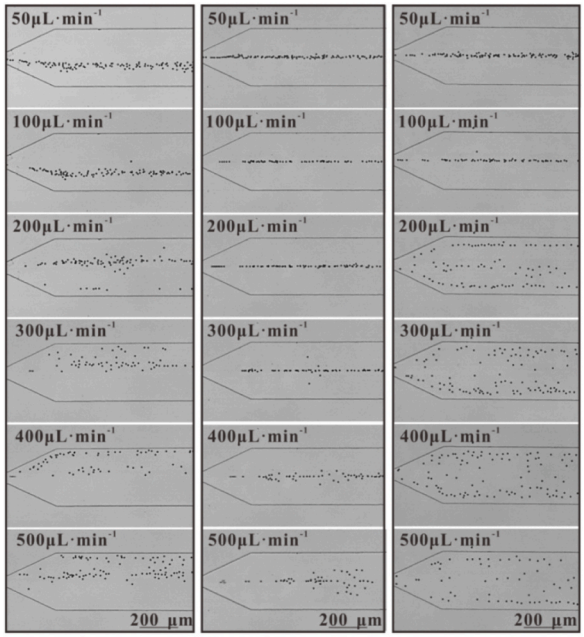

Fig. 5. 10 μm Particle distribution diagram of m particles at the outlet of microchannels with different angular structures. (a) Particle distribution at the microchannel exit for 10 μm particles under unilateral sharp angle structure distribution (b) Particle distribution at the microchannel exit for 10 μm particles under symmetric sharp angle structure distribution. (c) Particle distribution at the microchannel exit for 10 μm particles under staggered sharp angle structure distribution.

become better than the inertial lift force. Because some particles in the center of the channel are pushed to both sides of the channel under the effect of the reverse Dean's drag force due to the staggered distribution of sharp angle structure, and continue to move to both sides of the channel under the influence of the secondary eddy current generated by the expansion sections on both sides of the channel, so the particle flow will be formed at the upper and lower walls of the channel.

In order to further explain the lateral movement behavior of particles in microchannels with different angular structures, this paper conducts numerical simulation on the flow field distribution in microchannels with different angular structures. The results are shown in Fig. 7.

As shown in Fig. 7 (a), in the channel with sharp angle symmetrical distribution, the streamline is symmetrically distributed along the center of the channel, so the induced bending streamline at the symmetrical sharp angle structure will become gentle, resulting in the Dean drag force level caused by the bending streamline is far less than the inertial lift force, and the particles are in an inertial equilibrium state under the action of inertial lift force, so the particles will be distributed in the center of the channel. As the flow increases to 300 μL min^{-1} or above, secondary vortex will appear in the expansion area on both sides of the sharp corner channel, which will slightly disturb the particle distribution and will not affect the migration of particle equilibrium position. In the channel with crisscross distribution on both sides of the sharp corner structure, the flow rate is 100 μL min^{-1}, the streamline at the sharp corner structure is severely curved, but an S-shaped curve is formed in the mainstream direction of the microchannel. At this time, the flow rate is small, and the particles are weakly affected by Dean's drag force. The particles originally located on both sides of the channel will balance in the center of the channel under the effect of inertial lift. When the flow increases to 300 μL min^{-1} or above, the strength and distribution area of the secondary vortex will increase accordingly, forming pressure on the main flow area, resulting in the fluid in the main flow direction being limited to a narrow range, the velocity gradient of the fluid becoming larger, and the Dean drag force on the particles will also increase. The reverse Dean drag force caused by the staggered sharp angle structure will push the particles in the center of the channel to the secondary vortex in the expansion area on both sides, so that the particles will be distributed on both sides of the channel. The streamline near the sharp corner structure bends slowly. As shown in Fig. 7 (b), among the channels with symmetrical distribution of sharp corners and the low flow rate of 50 μL min^{-1}, four symmetrical vortices will appear on the cross section at the center of the sharp corner structure, and the particles will be focused at the center of the channel under the effect of Dean vortex. The flow field and streamline distribution on the cross section at the center of the sharp corner structure are consistent in the channels with one side distribution and two sides staggered distribution of the sharp corner structure, indicating that the effect of these two channels at the sharp corner structure is the same.

Then the influence of the shape of the single side distributed variable cross-section microstructure on the inertial transport behavior of particles is studied. The microstructure shapes are respectively sharp angle structure, arc structure, semicircle structure and rectangular structure.

Under different flow conditions, The distribution of 10 μm particles at the outlet of channels with different microstructures is shown

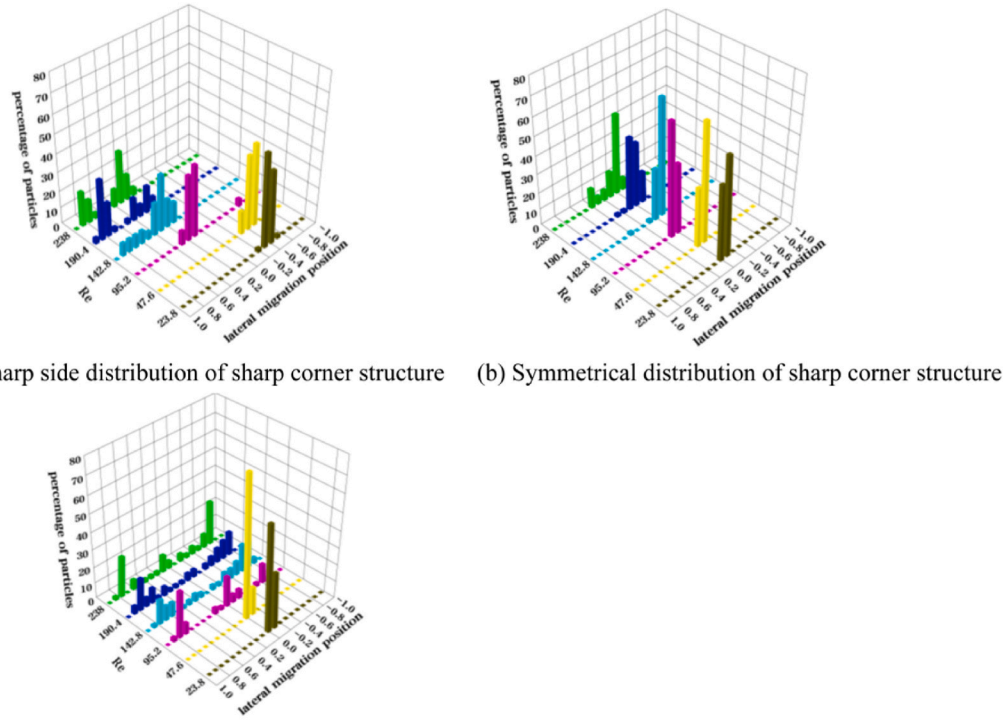

Fig. 6. Under different flow conditions, 10 μm Particle distribution histogram of m particles at the outlet of microchannels with different angular structures. (a) Bar graph showing the distribution of 10 μm particles at the microchannel exit under unilateral sharp angle structure distribution at different flow rates. (b) Bar graph showing the distribution of 10 μm particles at the microchannel exit under symmetric sharp angle structure distribution at different flow rates. (c) Bar graph showing the distribution of 10 μm particles at the microchannel exit under staggered sharp angle structure distribution at different flow rates.

in Fig. 8, and the particle distribution histogram at the outlet of channels with different variable cross-section microstructures is shown in Fig. 9. It can be seen from Fig. 8(a–d) and Fig. 9(a–d) that the lateral migration of these micro structured particles with variable cross section has a common feature, that is, with the increase of flow rate, the particles migrate from the micro structured side to the wall of the unstructured side. Specifically, at the low flow rate of 50 μL min^{-1} ($R_e = 23.8$) shown in Fig. 8(a–d) and Fig. 9(a–d), the particles balance below the channel (microstructure side). This is because the microstructures with different variable cross sections can induce curved streamline, thus triggering Dean's drag force. The balance position near the relative position of one side of the microstructure is - 0.4 to achieve force balance. With the increase of flow rate, particles begin to migrate above the channel (straight wall side), and multiple streams of particle flow begin to appear in the channel. With the increase of flow rate, Dean's drag force is strengthened. At this time, Dean's drag force is slightly stronger than inertial lift force, and the lateral force on particles is not in equilibrium, but the effect of Dean's drag force is not enough to drive all particles to the straight wall side, so multiple streams of particle flow appear in the channel, And when the flow rate increases to a certain extent, the effect of particles subjected to Dean's drag force is far better than that of inertial lift, pushing all particles to the straight wall above the channel. At this time, the particles form a new equilibrium position near the relative position of 0.8 on one side of the straight wall, and the particles return to a stable state of equilibrium position. However, different microstructure shapes also have differences. It can be seen that when the flow rate is 300 μL min^{-1} ($R_e = 142.8$) or higher than that shown in Fig. 8(a–d) and Fig. 9(a–d), in the angular structure microchannel, the particles are mainly distributed on the side where the channel center is inclined to the straight wall, while in other microstructure channels, the main flow of particles has reached the place near the straight wall. This is because there is a section of area with sharp change of section slope in the rectangular micro structure area, and the momentum of fluid flowing through these structures will change more, which will lead to greater Dean drag force. However, the cross section of the sharp corner structure area changes linearly, resulting in a small change in fluid momentum, and the sharp change in the cross section will more easily cause the velocity mismatch of the fluid in the central area and the near wall area of the microstructure in the downstream direction, resulting in greater secondary flow, which will cause greater disturbance to the lateral migration of particles. It can be seen that the particle agglomeration is more likely to occur at the outlet of the channel of rectangular, fan-shaped and semicircular structures, And small strands of particles will appear below the channel.

In order to further explain the lateral movement behavior of particles in micro channels with different variable cross-sections, this paper conducts numerical simulation on single-phase flow models in micro channels with different structures, and the simulation results are shown in Fig. 10.

Fig. 10 (a) shows that when the flow is 100 μL min^{-1}, the velocity distribution and streamline of the flow field in different variable

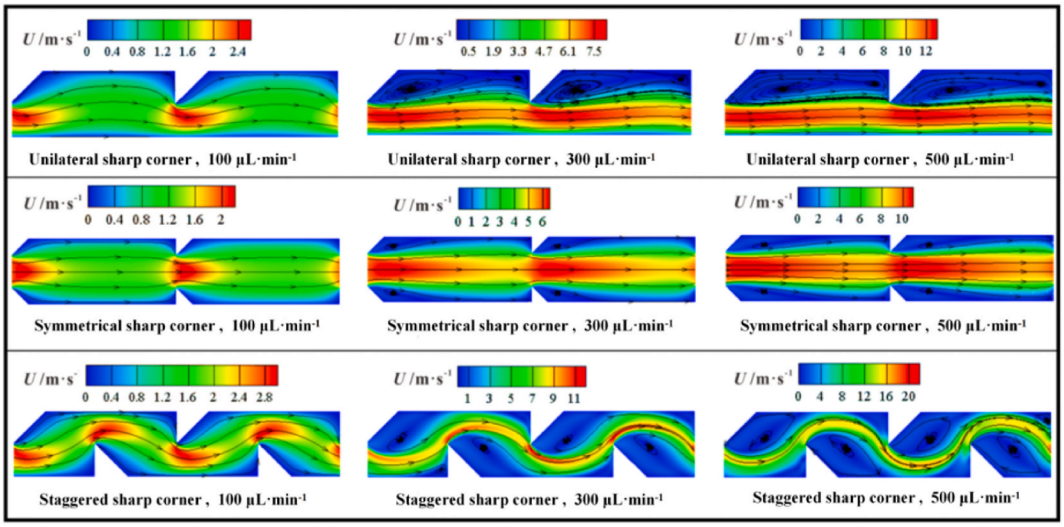

(a) Flow field and streamline diagram of channel section in flow direction

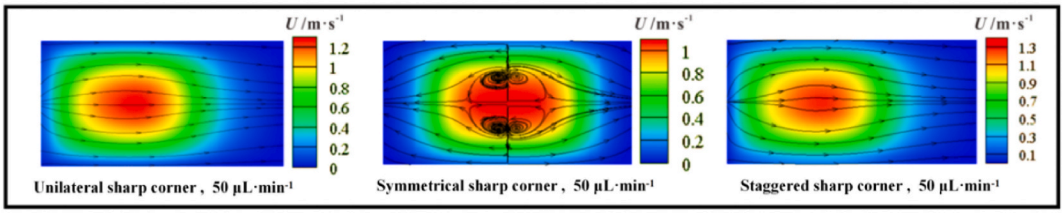

(b) Radial distribution velocity nephogram on the section at the center of sharp angle structure

Fig. 7. Numerical simulation diagram in microchannels with different angular structures. (a) Flow field and streamline diagrams at the channel cross-section for unilateral sharp angle structure, symmetric sharp angle structure, and staggered sharp angle structure under different flow rates along the flow direction. (b) Radial velocity distribution diagrams on the cross-section at the center of unilateral sharp angle structure, symmetric sharp angle structure, and staggered sharp angle structure.

cross-section microstructures are similar, and the curvature of streamline induced by different microstructures is also similar. When the flow increases to 300 μL min^{-1}, the velocity distribution of the flow field in different variable cross-section micro structure channels is consistent, but at this time, secondary vortex will appear in the expansion area of the channel, and strong secondary flow will appear in the semicircular structure, arc structure and rectangular structure. This is because there is a section of the micro structure area with a sharp change in section slope, The rapid change of the section will more easily cause the velocity mismatch of the fluid in the downstream direction between the central area and the micro structure near the wall area, which will result in a larger secondary flow. The section of the sharp corner structure area changes linearly, the speed of section expansion is constant, and the velocity mismatch of the fluid in the central area and the sharp corner near the wall area in the downstream direction is small, which will cause a smaller secondary flow. Fig. 10 (b) The radial velocity distribution cloud diagram on the cross section at the center of different microstructures shows that when the flow rate is 50 μL min^{-1}, it can be seen that the radial velocity distribution of different variable cross-section structures is consistent, but there will be two symmetrical Dean vortices on the section of semicircle structure and rectangular structure, and the particles will gather at the center of the vortex under the effect of Dean vortex, so that they can be arranged better.

Based on the results and discussions presented, unlike in straight channels, particle motion within microchannels with varying cross-sectional geometries is primarily regulated by inertial lift, viscous drag, and inertial centrifugal forces. The inertial lift tends to guide particles to an inertial equilibrium position near the channel center, while viscous drag and inertial centrifugal forces modify this equilibrium position. At low flow rates, the inertial equilibrium position of particles shifts towards the taper side to a relative position of 0.4 under the lateral component of viscous drag. At high flow rates, the inertial equilibrium position shifts towards the straight wall side to a relative position of 0.8 under the influence of inertial centrifugal force. The migration pattern of the equilibrium position changes with different arrangements of taper structures. With increasing flow rate, particles migrate from the channel center towards both sides in a staggered arrangement; in a symmetrical arrangement, particles consistently balance at the channel center. The migration pattern of equilibrium positions in other varying cross-sectional microstructures is similar to that in taper structures. For studies on microstructures of different shapes, the cross-sectional area in the taper structure region changes linearly, resulting in smaller changes in fluid momentum and weaker secondary flows, making the effects of flow rate changes less sensitive and more stable. Conversely, channels with rectangular, fan-shaped, and semicircular geometries generate stronger secondary flows, leading to a higher

Fig. 8. 10 μm Particle distribution diagram of m particles at the outlet of channels with different microstructure shapes. (a) Particle distribution diagram at the channel exit for 10 μm particles with sharp angle microstructure shape. (b) Particle distribution diagram at the channel exit for 10 μm particles with arc-shaped microstructure. (c) Particle distribution diagram at the channel exit for 10 μm particles with semicircular microstructure shape. (d) Particle distribution diagram at the channel exit for 10 μm particles with rectangular microstructure shape.

tendency for particle aggregation at the outlet and the appearance of small streams of particles at the bottom of the channel. This study offers guidance for the design of microchannels used for particle enrichment by investigating the geometric shapes of microstructures.

4.2. Research on inertial motion of particles in linear microstructured channels based on dissipative particle dynamics

DPD is a new mesoscopic method. As a bridge between macro scale and micro scale, it not only solves the problem that macro scale cannot reflect the micro characteristics of particle movement, but also improves the computational efficiency at the micro molecular level. Although DPD has been successfully applied to the simulation of various micro scale flow problems, there are still many unsolved problems hindering the wide use of this efficient calculation method, among which the solid-liquid boundary treatment of variable geometry channel structure is a challenge. Therefore, this summary will study the solid wall boundary treatment method applicable to the channel with variable cross-section structure, and develop a dissipative particle dynamics model suitable for the liquid-solid two-phase flow in the straight channel with variable cross-section microstructure.

DPD simulation of particle motion in microchannels with symmetrical sharp corners driven by different pressures is carried out in this paper and the microchannel model in DPD simulations is illustrated in Fig. 11(a and b). In order to improve computing efficiency and save computing resources, the real channel size is reduced by 2.5 times in the same scale in this simulation. The schematic diagram of the channel model is shown in Fig. 12. The simulation area is $-40 \leq x \leq 40$, $-6 \leq y \leq 6$, $-16 \leq z \leq 16$. Periodic boundaries are used in the x and y directions, and frozen two layers of DPD particles are used as the upper and lower walls in the z direction. This paper studies the migration of particles in the z direction (lateral). Fluid particles are arranged according to the position of face centered cubic, and solid particles are also arranged in face centered cubic to form a spherical structure with a diameter of 4. The whole simulation system is composed of 130560 DPD particles, including 140 particles, 7680 particles on the wall, 3276 particles with sharp corners and 119464 fluid particles.

By giving the fluid particles a horizontal driving force f to correspond to the pressure driving effect of the injection pump in the experiment, the particles will migrate laterally under the drive of the fluid particles, and finally the particles will appear at a fixed position, that is, the equilibrium position of the particles, after stabilizing, and then compare with the experiment. The interaction parameter between fluid particles and wall particles is set as 0.9375, and the interaction parameter between fluid particles and

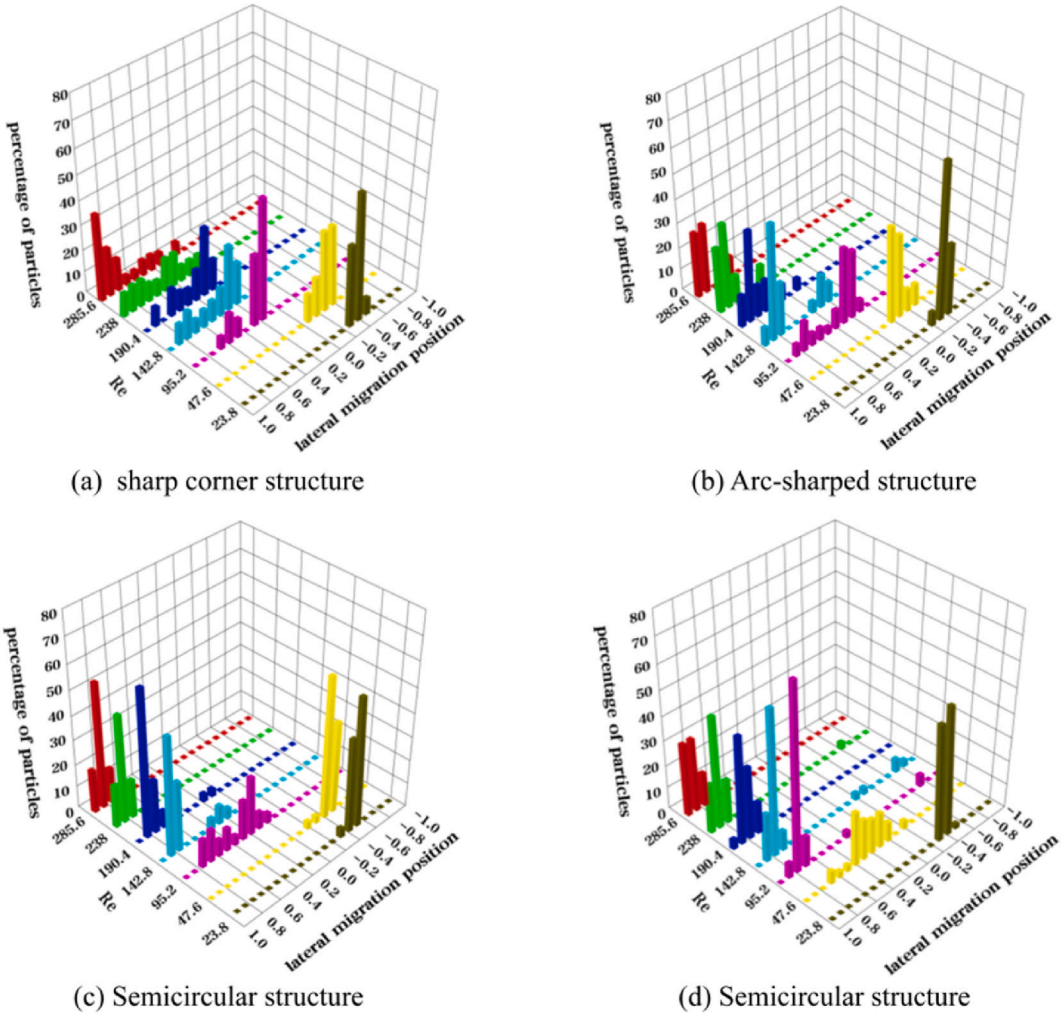

Fig. 9. Under different flow conditions, 10 μm Particle distribution histogram of m particles at the outlet of channels with different microstructure shapes. (a) Bar graph of the particle distribution at the microchannel exit for 10 μm particles with sharp angle microstructure shape under different flow rates. (b) Bar graph of the particle distribution at the microchannel exit for 10 μm particles with arc-shaped microstructure under different flow rates. (c) Bar graph of the particle distribution at the microchannel exit for 10 μm particles with semicircular microstructure shape under different flow rates. (d) Bar graph of the particle distribution at the microchannel exit for 10 μm particles with rectangular microstructure shape under different flow rates.

particles with symmetric sharp corner structure and between particles and particles with symmetric sharp corner structure is empirically set as 200f times of the conservative force coefficient a_{ij} of fluid particles, with time step Δt is set to 0.01, the system first relaxes 5000 steps to make the system stable, then applies the driving force f in the x direction (horizontal direction) to each fluid particle, and then runs 120000 steps to make the particle movement stable, and then statistically averages the relevant physical quantities of the stabilized particles.

This paper first verified the equilibrium position of particles at different initial release positions after final stabilization when the horizontal driving force f of fluid particles given by the model is 0.05. The results are shown in Fig. 12. It can be seen that no matter where the particles are released from the symmetric angular structure microchannel, they will be distributed near the center of the channel after final stabilization. Therefore, the final equilibrium position of particles is independent of the initial release position, which is consistent with our objective understanding. The final equilibrium position of particles is consistent with the experimental results in this paper.

This paper verifies the equilibrium position of the particle in the center of the channel after the final stability when the model gives different horizontal driving forces f to the fluid particles. The results are shown in Fig. 13. With the increase of the horizontal driving force from 0.03 to 0.09, the particles are always balanced near the center of the channel, but with the increase of the driving force, the balance position of the particles will shift to the upper part of the channel. It should be noted that, because the rough sphere model selected in this paper is a single spherical particle, the upward shift of the balance position at this point should be interpreted as that the distribution bandwidth of particles in the center of the channel will become larger, It can also be interpreted as fluctuation near the

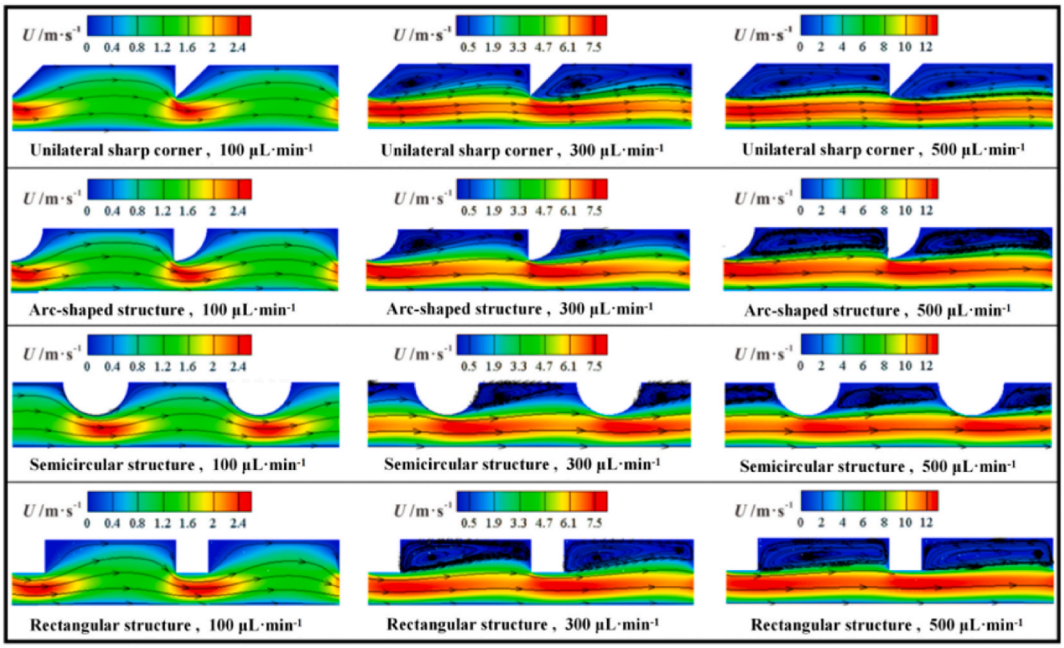

(a) Flow field and streamline diagram of channel section in flow direction

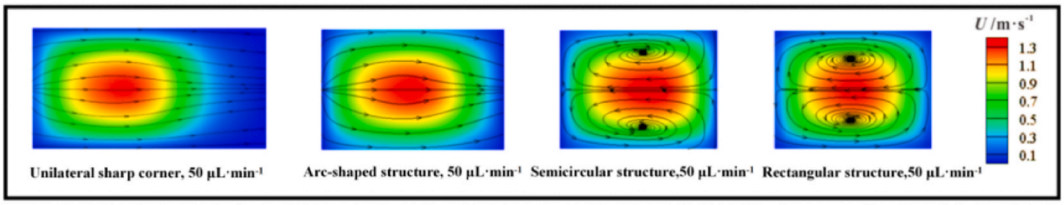

(b) Cloud Chart of Radial Velocity Distribution on Sections at the Center of Different Variable Section Structures

Fig. 10. Numerical simulation diagram in channels with different microstructure shapes. (a) Flow field and streamline diagrams at the microchannel cross-section for sharp angle microstructure, arc-shaped microstructure, semicircular microstructure, and rectangular microstructure under different flow rates along the flow direction. (b) Radial velocity distribution diagrams on the cross-section at the center of sharp angle microstructure, arc-shaped microstructure, semicircular microstructure, and rectangular microstructure.

center of the channel. This is consistent with the lateral migration rule and change trend of particles in the symmetric sharp channel experiment in this paper, but there are still some differences in quantitative comparison. However, it can be considered that the dissipative particle dynamics model of fluid solid interaction in this paper is reliable in studying the lateral migration of particles in symmetric angular structure channels driven by pressure. Therefore, the dissipative particle dynamics model established in this paper is applicable to microstructures with different distribution forms.

Since the dissipative particle dynamics model of particle fluid solid interaction in the variable cross-section micro structure channel established in this paper has a good agreement with the experimental results on the lateral migration rule and change trend of particles, the mesoscopic dissipative force sub dynamics method can reveal the lateral migration behavior of particles to a certain extent. In order to obtain the reasons for the lateral migration of particles, this section will analyze the lateral force and movement of particles in the variable cross-section microstructure channel.

In this paper, the forces acting on particles at different initial positions in the z direction (lateral direction) after different horizontal driving forces f are applied to fluid particles are calculated. In order to eliminate the influence of the random movement of particles in the simulation process on the force magnitude of particles at different positions, this paper will clear after recording the force on particles in each iteration process, so that particles can not move in the z direction, and can only be affected by the effect of fluid particles on particles. DPD simulation parameters are the same as those in the previous section, with time step Δt is set to 0.01, the system first relaxes 5000 steps to make the system stable, then applies the driving force f in the x direction (horizontal direction) to each fluid particle, and then runs 150000 steps to ensure that the fluid particle flow is stable. After reaching the stable state, the force of each step in the z direction of particles is statistically averaged. The force on particles at different positions after statistical averaging is shown in Fig. 14. In the figure, a positive value indicates that the direction of the force points above the channel (on the side of the straight wall), and a negative value indicates that the direction of the force points below the channel (on the side of the microstructure).

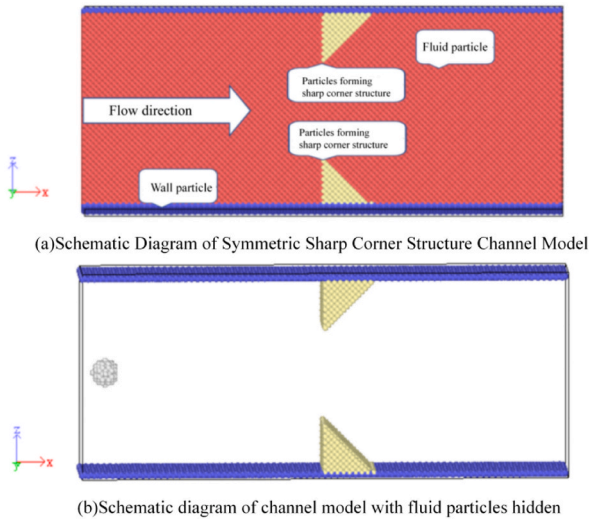

Fig. 11. Schematic diagram of DPD model of symmetric sharp angle structure channel. (a)Schematic Diagram of Symmetric Sharp Corner Structure Channel Model. (b)Schematic diagram of channel model with fluid particles hidden.

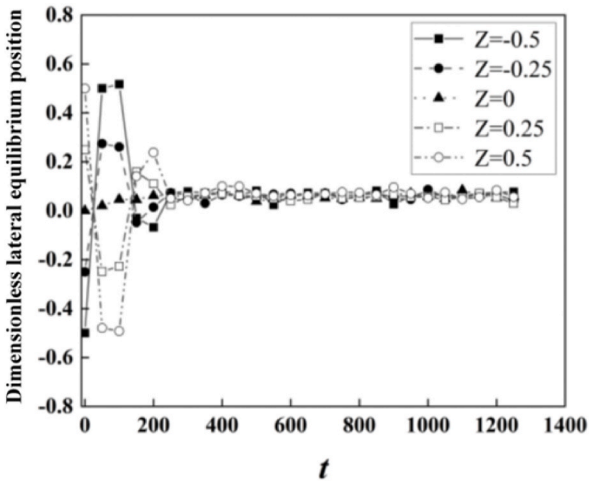

Fig. 12. When the horizontal driving force f of fluid particles is 0.05, the particle motion trajectories at different initial positions in the symmetric sharp corner structure.

Fig. 14 (a) shows that in the single side sharp corner structure channel, when the horizontal driving force is 0.05, it can be seen that the force on the force curve near - 0.4 is 0, and the force on both sides near this position is in the opposite direction, indicating that the force on the particles here is balanced, so the particles will form a balanced position here. The force on the particles on both sides of the channel is close to zero, but the two positions are not in force balance, just because the fluid particles in the low velocity area on both sides of the channel have a weak effect on the particles. You can also see the particles below the balance position. The force exerted by the fluid particles on them points above the channel, and the force exerted by the fluid particles on them points below the channel. Therefore, the particles on both sides of the balance position will migrate to the balance position under the action of the fluid particles. Finally, the particles will be distributed at the balance position. With the increase of driving force, the force trend of particles is the same. It can be seen that for particles at different positions in the channel, the force exerted by the fluid particles on them is pointing above the channel (on the side of the straight wall), and the particles will migrate above the channel under the force of the fluid particles. With the increase of the horizontal driving force, the lateral force exerted on the particles will also increase, and the particles will migrate faster above the channel under the greater force, Finally, reach the balance position above the channel faster. It can also be seen that with the increase of horizontal driving force, the force on particles near 0.8 position is close to 0, indicating that with the increase of horizontal driving force, the new equilibrium position of particles will appear near 0.8 position above the channel.

Fig. 14 (b) shows that in the symmetric sharp corner structure channel, when the horizontal driving force is less than 0.07, the force on the particles at the center of the channel is 0, and the force on the particles at both sides of the center is opposite, indicating that the

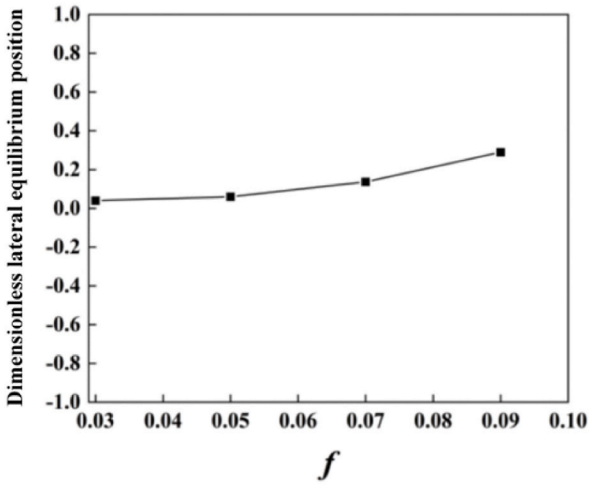

Fig. 13. Equilibrium position of particles in symmetric sharp channel when different horizontal driving forces f are applied to fluid particles.

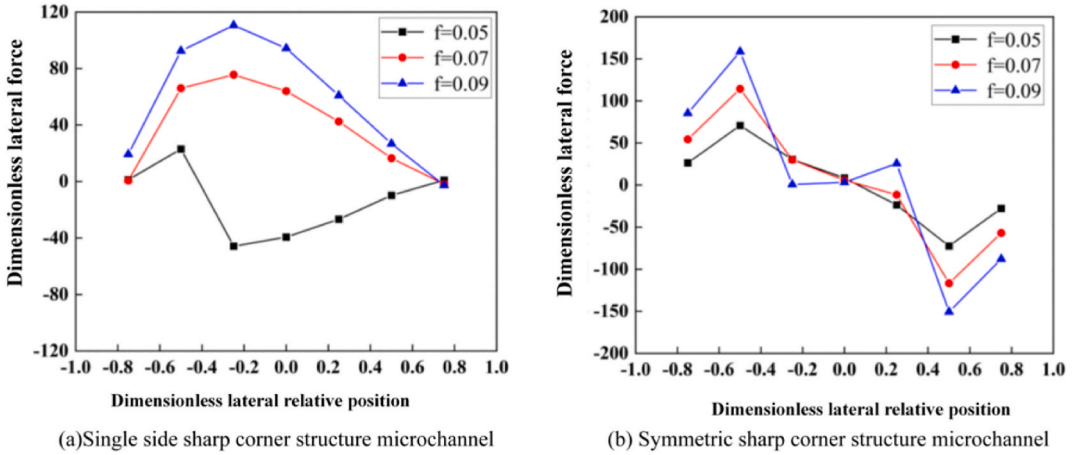

Fig. 14. Lateral Forces on Particles at Different Positions in Different Microstructure Channels when Different Horizontal Driving Forces f are Applied to Fluid Particles. (a) Lateral force diagram of particles in a unilateral sharp angle structure microchannel at different dimensionless lateral relative positions. (b) Lateral force diagram of particles in a symmetric sharp angle structure microchannel at different dimensionless lateral relative positions.

force on the particles at the center of the channel is always in equilibrium, that is, the equilibrium position of the particles is always at the center of the channel, and the particles below the channel can also be seen, The force exerted by fluid particles on it points to the upper part of the channel and the particles above the channel. The force exerted by fluid particles on it points to the lower part of the channel. Therefore, the particles on both sides of the channel will migrate to the center of the channel under the action of fluid particles. Finally, the particles will be distributed in the center of the channel after reaching equilibrium. But we can see that as the horizontal driving force increases to 0.09, the force curve of particles appears zero at the center of the channel, and the particles on both sides will move toward the center of the channel under the force of the two sides pointing to the center of the channel. However, at this time, the force curve of particles also appears a zero at both sides near the center of the channel, and a small part of particles in the center of the channel will fluctuate at the zero positions on both sides under the action of fluid particles, As a result, the distribution bandwidth of particles in the center of the channel is increased, but the additional particles on both sides of the zero point are subject to weak forces, which will only cause particles to fluctuate in the center of the channel, and will not modify the particle equilibrium position in the center of the channel, which is also consistent with our experimental results.

In conclusion, the force curve of particle lateral migration obtained in this paper is consistent with the rule and trend of particle lateral migration, so it also explains the behavior of particle lateral migration in the microstructure channel from a mesoscopic perspective.

Based on the simulation study described, we effectively tackled the challenge of handling complex, varying cross-sectional geometries with solid boundaries in dissipative particle dynamics (DPD) by freezing DPD particles to form microstructural regions and then increasing the conservative force coefficient of the particles in these regions. This approach introduced an interaction zone that

only involves repulsive forces, offering a viable solution to the difficulties associated with modeling fixed-wall boundaries in DPD methods. By comparing with experimental results, the lateral motion patterns and trends of particles closely matched the experiments, demonstrating that our developed DPD model for particle-fluid interactions within microstructured channels can reveal the mesoscale dynamics of liquid-solid two-phase flow and particle motion within microchannels.

5. Conclusion

In this study, we systematically investigated the impact of structural attributes on the inertial migration behavior of particles within straight microchannels, with a specific focus on the effects of microstructure shapes and their arrangements. The motion of particles in straight microchannels with various cross-sectional microstructures is predominantly governed by inertial lift forces, viscous drag, and inertial centrifugal forces. We found that the equilibrium position induced by inertial lift is modified by the combined effects of viscous drag and inertial centrifugal forces. Depending on the arrangement of sharp-angled microstructures, the migration pattern of the equilibrium position can vary significantly. Our observations indicated that particles in channels with one-sided sharp-angled microstructures migrate towards the angled side at a relative position of 0.4 under low flow rates, and towards the straight wall side at a relative position of 0.8 under high flow rates. The migration pattern of the equilibrium position changes with different arrangements of sharp-angled structures, with particles achieving equilibrium at the channel center only when sharp-angled microstructures are symmetrically arranged on both sides. Our study on the shape of microstructures revealed that sharp-angled structures produce a more stable secondary flow compared to rectangular and semi-circular structures, preventing particle agglomeration at the outlet. Furthermore, this research delved into the application of dissipative particle dynamics (DPD) methods for the motion of inertial particles within straight channels featuring microstructures. We developed a DPD model tailored for particle-fluid interactions within microchannels with variable cross-sectional microstructures. By enhancing the conservative force coefficient among particles within the microstructured regions and introducing an interaction zone exclusively comprising repulsive components as the microstructure area, the simulation results achieved an equilibrium position deviation of less than 1 % compared to experimental values. This approach addresses the challenge of dealing with variable geometric shape wall boundaries in the dissipative particle dynamics methodology.

In conclusion, our findings provide a nuanced understanding of the role of microstructural design in influencing particle migration behaviors in microfluidic environments. The insights gained from this study offer valuable guidance for the design of microchannels aimed at particle enrichment and separation, enhancing the potential applications of microfluidic systems in biomedical and analytical fields.

Funding

National Natural Science Foundation of China (No.: 52076174 and 51476127)

CRediT authorship contribution statement

Hua Dong: Writing – review & editing, Validation, Supervision, Resources, Project administration, Conceptualization. **Longrun Huang:** Writing – original draft, Methodology, Investigation. **Liang Zhao:** Investigation, Formal analysis, Data curation.

Declaration of competing interest

The authors declare that they have no known competing financial interests or personal relationships that could have appeared to influence the work reported in this paper.

References

[1] A. Manz, N. Graber, H.M. Widmer, Miniaturized total chemical analysis systems: a novel concept for chemical sensing[J]. Sensors and Actuators, B: Chemical 1 (1–6) (1990) 244–248.
[2] R. Pol, F. Cespedes, D. Gabriel, Microfluidic lab-on-a-chip platforms for environmental monitoring, Trac-trends in Analytical Chemistry 95 (2017) 62–68.
[3] S.T. Sanjay, W. Zhou, M.W. Dou, et al., Recent advances of controlled drug delivery using microfluidic platforms, Adv. Drug Deliv. Rev. 128 (15) (2018) 3–28.
[4] C. Carrell, A. Kava, M. Nguyen, et al., Beyond the lateral flow assay: a review of paper-based microfluidics, Microelectron. Eng. 206 (1) (2019) 45–54.
[5] S. Sachdeva, R.W. Davis, A.K. Saha, Microfluidic point-of-care testing: commercial landscape and future directions, Front. Bioeng. Biotechnol. 8 (15) (2021) 602659.
[6] A.J. Mach, O.B. Adeyiga, D. Di Carlo, Microfluidic sample preparation for diagnostic cytopathology, Lab Chip 13 (6) (2013) 1011–1026.
[7] D.J. Beebe, G.A. Mensing, G.M. Walker, Physics and applications of microfluidics in biology, Annu. Rev. Biomed. Eng. 4 (1) (2002) 261–286.
[8] Yu Mingfen, Hongmei Zeng, Hua Zhang, et al., Research overview and application progress of microfluidic chip technology, Plant Prot. 40 (4) (2014) 1–8.
[9] A.S. Utada, E. Lorenceau, D.R. Link, et al., Monodisperse double emulsions generated from a microcapillary device, Science 308 (5721) (2005) 537–541.
[10] H. Gu, M.H. Duits, F. Mugele, Droplets formation and merging in two-phase flow microfluidics, Int. J. Mol. Sci. 12 (4) (2011) 2572–2597.
[11] Jinxia Mu, Xuefeng Yin, Application of microchannel reactor in synthesis reaction, Chemical Progress 20 (1) (2008) 60–75.
[12] M. Joanicot, A. Ajdari, Droplet control for microfluidics, Science 309 (5736) (2005) 887–888.
[13] X. Feng, Y. Ren, L. Hou, et al., Tri-fluid mixing in a microchannel for nanoparticle synthesis, Lab Chip 19 (17) (2019) 2936–2946.
[14] L. Jiang, Y. Zeng, Q. Sun, et al., Microsecond protein folding events revealed by time-resolved fluorescence resonance energy transfer in a microfluidic mixer, Anal. Chem. 87 (11) (2015) 5589–5595.
[15] A.S. Kastania, K. Tsougeni, G. Papadakis, et al., Plasma micro-nanotextured polymeric micromixer for DNA purification with high efficiency and dynamic range, Anal. Chim. Acta 942 (26) (2016) 58–67.

[16] T.Y. Lee, K. Hyun, S. Kim, et al., An integrated microfluidic chip for one-step isolation of circulating tumor cells, Sensor. Actuator. B Chem. 238 (2017) 1144–1150.
[17] A. Mahboubidoust, A. Ramiar, K. Sedighi, Design of an optimized ECCA microchannel for particle manipulation utilizing dean flow coupled elasto-inertial method, Adv. Powder Technol. 32 (5) (2021) 1688–1709.
[18] J. Nam, J. Yoon, H. Jee, et al., High-Throughput separation of microvesicles from whole blood components using viscoelastic fluid, Advanced Materials Technologies 5 (12) (2020) 2000612.
[19] G. Segre, A. Silberberg, Radial particle displacements in Poiseuille flow of suspensions, Nature 189 (4760) (1961) 209–210.
[20] Y.W. Kim, J.Y. Yoo, The lateral migration of neutrally-buoyant spheres transported through square microchannels, J. Micromech. Microeng. 18 (6) (2008) 065015.
[21] J.P. Matas, J.F. Morris, É. Guazzelli, Inertial migration of rigid spherical particles in Poiseuille flow, J. Fluid Mech. 515 (2004) 171–195.
[22] S.C. Hur, H.T.K. Tse, D. Di Carlo, Sheathless inertial cell ordering for extreme throughput flow cytometry, Lab Chip 10 (3) (2010) 274–280.
[23] J. Hansson, J.M. Karlsson, T. Haraidsson, et al., Inertial particle focusing in parallel microfluidic channels for high-throughput filtration[C]//Solid-State Sensors, in: Actuators and Microsysytems Conference (Transducers),2011 16th International, IEEE, 2011, pp. 1777–1780.
[24] P. Jae-Sung, S. Suk-Heung, J. Hyo-Il, Continuous focusing of microparticles using inertial lift force and vorticity via multi-orifice microfluidic channels, Lab Chip 9 (7) (2009) 939–948.
[25] M. Yilmaz, M. Cengiz, H. Kizil, et al., Geometry induced microparticles separation in passive contraction expansion straight channels[C]//ICQNM 2011, the Fifth International Conference on Quantum, Nano Micro Technol. (2011) 89–93.
[26] M.G. Lee, S. Choi, J. Park, Three-dimensional hydrodynamic focusing with a single sheath flow in a single-layer microfluidic device, Lab Chip 9 (21) (2009) 3155–3160.
[27] J. Zhang, M. Li, W.H. Li, et al., Inertial focusing in a straight channel with asymmetrical expansion-contraction cavity arrays using two secondary flows, J. Micromech. Microeng. 23 (8) (2013) 85023–85035.
[28] A.J. Chung, D. Pulido, J.C. Oka, et al., Microstructure-induced helical vortices allow single-stream and long-term inertial focusing, Lab Chip 13 (15) (2013) 2942–2949.
[29] D. Yuan, J. Zhang, R. Sluyter, et al., Continuous plasma extraction under viscoelastic fluid in a straight channel with asymmetrical expansion–contraction cavity arrays, Lab Chip 16 (20) (2016) 3919–3928.
[30] L.L. Fan, Y. Han, X.K. He, et al., High-throughput, single-stream microparticle focusing using a microchannel with asymmetric sharp corners, Microfluid. Nanofluidics 17 (4) (2014) 639–646.
[31] E.S. Asmolov, The inertial lift on a spherical particle in a plane Poiseuille flow at large channel Reynolds number, J. Fluid Mech. 381 (0) (1999) 63–87.
[32] S. Cho, H. Choi, J. Yoo, Direct numerical simulation of fluid flow laden with many particles, Int. J. Multiphas. Flow 31 (4) (2005) 435–451.
[33] P. Espanol, P. Warren, Statistical mechanics of dissipative particle dynamics, Europhys. Lett. 30 (4) (1995) 191.
[34] H. Liu, S. Jiang, Z. Chen, et al., Mesoscale study of particle sedimentation with inertia effect using dissipative particle dynamics, Microfluid. Nanofluidics 18 (5–6) (2015) 1309–1315.
[35] Y. Kong, C.W. Manke, W.G. Madden, et al., Simulation of a confined polymer in solution using the dissipative particle dynamics method, Int. J. Thermophys. 15 (6) (1994) 1093–1101.
[36] P. Malfreyt, D.J. Tildesley, Dissipative particle dynamics simulations of grafted polymer chains between two walls, Langmuir: The ACS Journal of Surfaces and Colloids 16 (10) (2000) 4732–4740.
[37] J.L. Jones, M. Lal, J.N. Ruddock, et al., Dynamics of a drop at a liquid/solid interface in simple shear fields: a mesoscopic simulation study, Faraday Discuss 112 (1) (1999) 129–142.
[38] D.C. Visser, H.C.J. Hoefsloot, P.D. Iedema, Comprehensive boundary method for solid walls in dissipative particle dynamics, J. Comput. Phys. 205 (2) (2005) 626–639.
[39] J. Haugen, J. Ziebarth, E.C. Eckstein, et al., Hydrodynamic and transport behavior of solid nanoparticles simulated with dissipative particle dynamics, Adv. Nat. Sci. Nanosci. Nanotechnol. 14 (2) (2023) 025006.
[40] J.H. Tan, T. Yamada, Y. Asako, et al., Study of self diffusion of nanoparticle using dissipative particle dynamics, Journal of Advanced Research in Numerical Heat Transfer 10 (1) (2022) 1–7.
[41] J. Wang, Y. Han, Z. Xu, et al., Dissipative particle dynamics simulation: a review on investigating mesoscale properties of polymer systems, Macromol. Mater. Eng. 306 (4) (2021) 2000724.
[42] H. Dong, X. Wu, L.L. Fan, et al., An improved dissipative particle dynamics method for the liquid-particle two-phase flow in microchannels, J. Micromech. Microeng. 33 (10) (2023) 105012.
[43] Guo, Dynamics of Two-phase and Multiphase flow[M], Xi'an Jiaotong University Press, Xi'an, 2002, pp. 484–490.
[44] D. Huang, J.X. Man, D. Jiang, et al., Inertial microfluidics: recent advances, Electrophoresis 41 (24) (2020) 2166–2187.
[45] X. Mao, S.S. Lin, C. Dong, Single-layer planar on-chip flow cytometer using microfluidic drifting based three-dimensional (3D) hydrodynamic focusing, Lab Chip 9 (11) (2009) 1583–1589.
[46] A.A.S. Bhagat, S.S. Kuntaegowdanahalli, I. Papautsky, Enhanced particle filtration in straight microchannels using shear-modulated inertial migration, Phys. Fluids 20 (10) (2008) 101702.
[47] Y.W. Kim, J.Y. Yoo, Three-dimensional focusing of red blood cells in microchannel flows for bio-sensing applications, Biosens. Bioelectron. 24 (12) (2009) 3677–3682.
[48] Y. Ruey-Jen, H. Hui-Hsiung, W. Yao-Nan, et al., A hydrodynamic focusing microchannel based on micro-weir shear lift force, Biomicrofluidics 6 (3) (2012) 034110.
[49] Li, Jiang, Study on the rising rule of small wooden balls in solid-liquid two-phase flow and Magnus force measurement, Journal of Dalian University of Technology 51 (5) (2011) 653–657.
[50] H. Amini, W. Lee, D. DiCarlo, et al., Inertial microfluidic physics, Lab Chip 14 (15) (2014) 2739–2761.
[51] D.C. Duffy, J.C. McDonald, O.J.A. Schueller, et al., Rapid prototyping of microfluidic systems in poly, Anal. Chem. 70 (23) (1998) 4874–4984.